SPARSE HYPERSPECTRAL UNMIXING WITH SPATIAL DISCONTINUITY PRESERVATION

Shaoquan Zhang[1]*, Jun Li*[1]*, Zebin Wu*[2] *and Antonio Plaza*[3]

[1]Guangdong Key Laboratory for Urbanization and Geo-Simulation,
School of Geography and Planning, Sun Yat-sen University, Guangzhou, China.
[2]School of Computer Science and Engineering, Nanjing University of Science and Technology, China.
[3]Hyperspectral Computing Laboratory, University of Extremadura, Caceres, Spain.

ABSTRACT

Sparse unmixing and sparse representation are known to be effective for improving the interpretation of remotely sensed hyperspectral images. Classic methods for incorporating spatial information into spectral unmixing assume that the abundances of the pixels are smooth and fall into a homogeneous region shared by the same endmembers and their corresponding fractional abundances. Sometimes this assumption does not hold in practice, as images contain abrupt changes in endmember abundances, i.e., abundance maps are often spatially heterogeneous. To address this limitation, in this work we propose a novel sparse unmixing framework with discontinuity preservation which aims at preserving the spatial heterogeneity present in abundance maps. In the proposed framework, the Sobel operator is used to characterize such discontinuities. Our experimental results, conducted using both simulated and real hyperspectral data sets, indicate that the introduction of a discontinuity preserving strategy on sparse unmixing formulations is beneficial to preserve the spatial heterogeneity present in the abundance maps. We exploit this information effectively to improve abundance estimation.

Index Terms— Discontinuity preserving, spatial heterogeneity, sparse unmixing, hyperspectral imaging.

1. INTRODUCTION

Due to the insufficient spatial resolution of imaging spectrometers and the spatial complexity of natural scenes, pixels in remotely sensed hyperspectral images are likely to be formed by a mixture of pure spectral constituents (*endmembers*) rather than a single substance [1]. Spectral unmixing was proposed to deal with the problem. It aims at estimating the fractional abundances of the pure spectral signatures (endmembers) in each mixed pixel of the scene [2]. Under the linear spectral mixture model (LSMM), techniques based on extracting the endmembers directly from the scene have faced difficulties related with the unavailability of pure signatures in the image data. To overcome this limitation, sparse unmixing [3] has been developed as a semi-supervised approach in which mixed pixels are expressed in the form of linear combinations of a number of pure spectral signatures from a large spectral library that is known in advance. Sparse unmixing aims at finding the optimal subset of endmembers to represent the pixels in a hyperspectral image.

During the last decade, the integration of spatial-contextual information has proved to be an effective way to improve unmixing accuracy in spectral unmixing formulations [4]. The proposed methods for incorporating spatial information in abundance estimation, such as SUnSAL-TV [5] and ESC [6], assume that the abundances of the pixels are smooth and fall into a homogeneous region. Such uniform smoothness assumption implies that smooth abundance transitions happen everywhere in the scene. However, this assumption rarely holds in practice. Specifically, hyperspectral data are often characterized by low spatial resolution and high spectral resolution. As a result, endmember abundances smoothly are expected to exhibit spatial discontinuities [7]. Moreover, abrupt changes of abundances are similar to region edges in image segmentation, which are known to happen naturally in remotely sensed scenes [8]. Furthermore, even in the spatial neighborhood of pixels, most of the endmember fractional abundance values are expected to be different. This indicates that abundance maps are largely heterogeneous. As a result, the principle of uniform smoothness is violated as discontinuities related with abrupt endmember abundance changes are present in the scene. It is necessary to develop new strategies to preserve the heterogeneity of pixels in abundance maps for spectral unmixing purposes.

Recently, edge preserving filtering [9] has become a very active research topic in hyperspectral image processing. This strategy has been successfully applied for image classification [10, 11] and superresolution [12]. In [10] and [11], it was shown that classification methods can improve their accuracy significantly by the incorporation of edge preserving filtering. Inspired by edge preserving strategies in which textures can be smoothed while retaining sharp edges, and assuming that abundance maps are heterogeneous (especially in the object boundaries) we develop a new strategy for sparse hyperspectral unmixing which introduces spatial relaxation to accurately preserve the edges of abundance maps. In our newly developed method, edge detection is performed by means of a Sobel operator, which is used to characterize the discontinuities of the abundance maps. As demonstrated by our experimental results with both synthetic and real hyperspectral data sets, the proposed strategy can preserve the heterogeneity of abundance maps by including edge information into the sparse unmixing process.

2. SPARSE UNMIXING

The linear model assumes that the spectral response of a pixel is given by a linear combination of the endmembers present in the pixel. Sparse unmixing finds a linear combination of endmembers for an observed pixel from a large spectral library:

$$\mathbf{y} = \mathbf{A}\mathbf{x} + \mathbf{n} \tag{1}$$

where $\mathbf{y}$ denotes a $L \times 1$ pixel vector of the observed hyperspectral data, L denotes the number of bands, $\mathbf{A} \in \mathbb{R}^{L \times m}$ is a large spectral library, m is the number of spectral signatures in $\mathbf{A}$, $\mathbf{x}$ denotes the abundance vector corresponding to library $\mathbf{A}$, and $\mathbf{n}$ is an $L \times 1$ vector collecting the errors affecting the measurements at each spectral band. As the number of endmembers involved in a mixed pixel

is usually very small when compared with the size of the spectral library, the vector of fractional abundances $\mathbf{x}$ is sparse. Due to the physical meaning of the fractional abundances, the vector $\mathbf{x}$ is subject to nonnegativity ANC) and sum-to-one constraint (ASC). With these considerations in mind, the unmixing problem can be formulated as an $\ell_2 - \ell_0$ norm optimization problem. However, the $\ell_2 - \ell_0$ norm optimization problem is nonconvex and difficult to solve [13]. The sparse unmixing algorithm via variable splitting and augmented Lagrangian (SUnSAL) [3] was proposed to address this problem, it uses the $\ell_2 - \ell_1$ norm to replace the $\ell_2 - \ell_0$ norm. Then the collaborative SUnSAL (CLSUnSAL) [14] was developed under the assumption that all pixels in a hyperspectral image share the same active set of endmembers.

To improve the unmixing results further, some methods have been proposed to exploit spatial-contextual information under the sparse regression framework. For example, SUnSAL-TV [5] includes a total variation (TV) regularizer to promote spatial homogeneity among neighboring pixels. However, SUnSAL-TV may lead to oversmoothness and blurred boundaries. In real scenarios, fractional abundances exhibit heterogeneity and sharp transitions (especially in the object boundaries). According to this, if the results obtained are over-smoothed, they would lead to inaccurate proportion estimations. In the following we present a methodology to address this issue by introducing the concept of discontinuity preservation in sparse unmixing.

3. A NEW DISCONTINUITY PRESERVING STRATEGY FOR SPARSE UNMIXING

In order to illustrate the heterogeneity of abundance maps, we use an urban hyperspectral data set with ground-truth [8], which contains 307×307 pixels with a spatial resolution of $2m$. In this image, there are 210 spectral bands ranging from 400 to 2500 nm, resulting in spectral resolution of $10nm$. The ground-truth contains four endmembers and their corresponding true fractional abundances are known, as shown in Fig. 1. From a statistical point of view, the nonzero numbers of the four abundance maps are 56501,74892, 60582 and 59289, respectively. We set up four different thresholds (0.001, 0.01, 0.05, 0.1) for the difference between two adjacent pixels. Fig. 2 shows the difference values between two adjacent pixels that are greater than 0.001, 0.01, 0.05, 0.1, respectively. It can be seen from Fig. 2 that, no matter the scenario considered, the number of adjacent pixels that exhibit a significant difference in abundance values is very high. This reveals that there are significant differences between adjacent pixels, which confirms our introspection that abundance maps are largely heterogeneous. Based on aforementioned observation, it is very important to preserve the heterogeneity of abundance maps, especially in the boundaries of image objects. In this work, we integrate spatial information into the sparse unmixing formulation to preserve the heterogeneity of abundance maps via a discontinuity preserving method.

Here, we introduce a discontinuity preserving strategy which smooths textures while retaining sharp edges in the estimated abundances by means of sparse unmixing. There are many approaches that have been developed in the literature for detecting edges, such as the cross operator by Roberts, the Prewitt operator, the Sobel operator, the Laplacian operator and the Canny operator. In this paper, the Sobel operator was used to detect the discontinuities in an image. The edge image ε is given by

$$\varepsilon = \exp(-\mathbf{sobel}(\mathbf{x})), \tag{2}$$

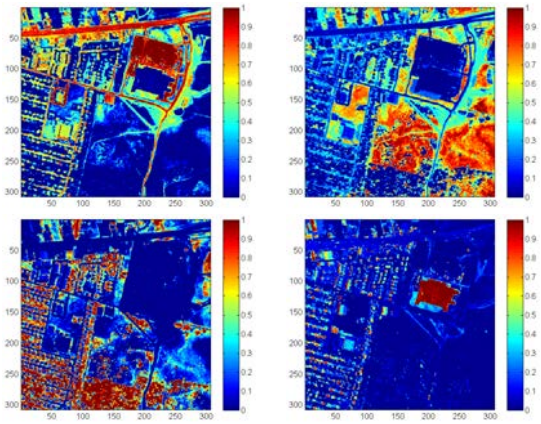

Fig. 1. True abundance maps of the four endmembers in the data.

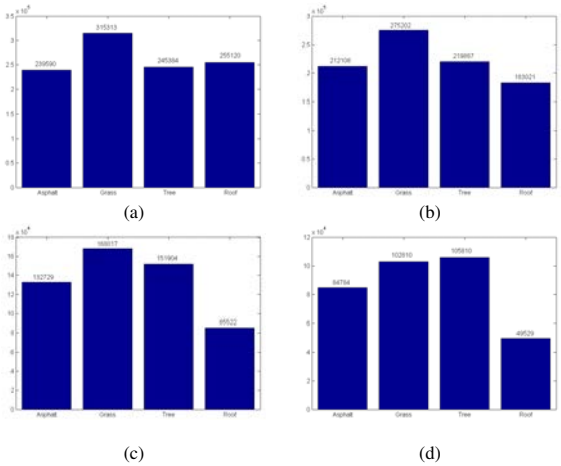

Fig. 2. A quantitative indication of the heterogeneity of abundance maps can be obtained by counting the number of times that the difference between two adjacent pixels in the abundance maps for the considered urban hyperspectral image is greater than: (a) 0.001, (b) 0.01, (c) 0.05, (d) 0.1. In all cases, the obtained numbers are high, suggesting abrupt transitions in the abundance values of adjacent pixels.

where $\mathbf{x}$ denotes the abundance matrix, sobel() denotes the Sobel filter, which detects the discontinuities in an image. The output at each pixel is either 0 or 1. In addition, to have a better interpretation of the edges, we considered the average of the results obtained by applying sobel() in two vertical and horizontal directions. By integrating ε into the sparse unmixing (e.g. SUnSAL, CLSUnSAL and SUnSAL-TV), we therefore can ensure the heterogeneity preservation of abundance maps.

4. RESULTS WITH SYNTHETIC DATA

The library that we use in our synthetic image experiments is a dictionary of minerals extracted from the United States Geological Survey (USGS) library. The library $\mathbf{A}$ contains $m = 240$ materials with $L = 224$ bands. We have simulated a 100×100-pixel synthetic datacube by randomly choosing nine signatures from $\mathbf{A}$. The fractional abundances are piecewise smooth, i.e., they are smooth with

sharp transitions, especially in the boundaries of image objects (a detailed description of the simulated data cube is available from [5]). After generating the datacube, it was contaminated with i.i.d. Gaussian noise, using three levels of the signal-to-noise ratio (SNR): 30, 40 and 50dB.

The signal-to-reconstruction error (SRE, measured in dB) is used to evaluate the unmixing accuracy. Let $\widehat{\mathbf{x}}$ be the estimated abundance of $\mathbf{x}$, and let $\mathbf{x}$ be the true abundance. The SRE can be computed as follows:

$$\text{SRE}(\mathbf{x}) = 10 \cdot \log_{10}(E(||\mathbf{x}||_2^2)/E(||\mathbf{x} - \widehat{\mathbf{x}}||_2^2)), \qquad (3)$$

where $E(\cdot)$ denotes the expectation function. The larger the SRE, the more accurate the unmixing. Furthermore, we use another indicator, i.e., the probability of success p_s, which is an estimate of the probability that the relative error power be smaller than a certain threshold. It is formally defined as follows: $p_s \equiv P(\|\widehat{\mathbf{x}} - \mathbf{x}\|^2/\|\mathbf{x}\|^2 \leq threshold)$. In our case, the estimation result is considered successful when $\|\widehat{\mathbf{x}}-\mathbf{x}\|^2/\|\mathbf{x}\|^2 \leq 3.16$ (5 dB). This threshold was demonstrated in [3].

Table 1 shows the SRE(dB) and p_s results achieved by the different tested algorithms, where DP denotes the discontinuity preserving strategy under different SNR levels. For all the tested algorithms, the input parameters have been carefully tuned for optimal performance. From Table 1, we can conclude that the inclusion of the discontinuity preserving strategy can improve unmixing performance in three different analysis scenarios. This reveals that the proposed strategy can preserve the heterogeneity of abundances for sparse unmixing purposes.

For illustrative purposes, Fig. 3 shows a graphical comparison of the performances of the considered unmixing algorithms. In this experiment, the datacube was contaminated with i.i.d. Gaussian noise having SNR of 40 dB. Since the abundance maps estimated for other endmembers exhibited similar behavior, we only report the results observed for abundance of one of them. The abundance maps displayed in Fig. 3 were obtained using optimal values for parameters λ (see Tables 1). The differences of the fractional abundances estimated by SUnSAL and SUnSAL-DP were calculated (also for CLSUnSAL and CLSUnSAL-DP, SUnSAL-TV and SUnSAL-TV-DP). From Fig. 3, it can be seen that the main differences can be observed at the edges of the abundance maps. This also reveals that the inclusion of a spatial term based on discontinuity preserving improves both the SUnSAL and the CLSUnSAL solutions. Furthermore, compared with SUnSAL-TV, the inclusion of the discontinuity preserving strategy which can relax the boundaries from oversmoothness or blurring. Despite the experiments with synthetic data are very encouraging, further experiments with real scenes are desirable. These will be reported in the following section.

5. RESULTS WITH REAL HYPERSPECTRAL DATA

As there is no spectral library for the aforementioned urban hyperspectral data, in this section, we resort to the well-known Airborne Visible Infrared Imaging Spectrometer (AVIRIS) Cuprite data set for evaluation of the proposed approach, which is available online in reflectance units [1]. The portion used in experiments corresponds to a 250×191-pixel subset of the scene, with 224 spectral bands in the range 0.4-2.5 μm and nominal spectral resolution of 10 nm. Prior to the analysis, bands 1-2, 105-115, 150-170, and 223-224 were removed due to water absorption and low SNR, leaving a total of 188 spectral bands. The spectral library used in this experiment is

[1] http://aviris.jpl.nasa.gov/html/aviris.freedata.html

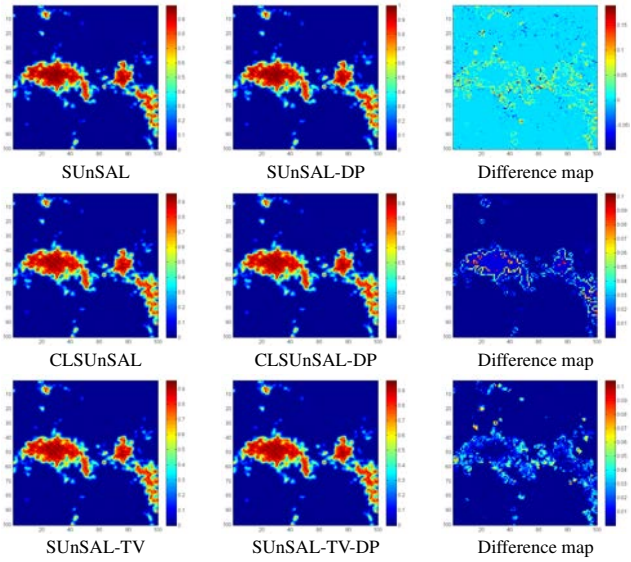

Fig. 3. The data set is contaminated with noise having SNR of 40 dB. Abundance maps obtained by different unmixing methods for endmember 9 and their difference maps.

the same library $\mathbf{A}$ used in our simulated experiments and the noisy bands are also removed from $\mathbf{A}$. For comparative purposes, we use a mineral map produced in 1995 by USGS, in which the Tricorder 3.3 software product [15] was used to map different minerals present in the Cuprite mining district. The USGS map serves as a good indicator for qualitative assessment of the fractional abundance maps produced by the different unmixing algorithms.

Fig.4 conducts a qualitative comparison between the classification maps produced by the USGS Tricorder algorithm and the fractional abundances estimated by CLSUnSAL, CLSUnSAL-DP and SUnSAL-TV, SUnSAL-TV-DP algorithms for three highly representative minerals in the Cuprite mining district (Alunite, Buddingtonite and Chalcedony). The differences of fractional abundances estimated by CLSUnSAL and CLSUnSAL-DP were calculated (same for SUnSAL-TV and SUnSAL-TV-DP). As shown in Fig. 4, both the CLSUnSAL-DP and SUnSAL-TV-DP exploit the proposed discontinuity preserving strategy to obtain better abundances at the edges of image objects. It is worth noting that the fractional abundance maps estimated by CLSUnSAL-DP, SUnSAL-TV-DP provide a higher similarity to the Tricorder maps. Thus, from a qualitatively perspective we can conclude that heterogeneity preservation exhibits the potential to improve the results obtained by sparse unmixing in real scenarios.

6. CONCLUSIONS AND FUTURE WORK

A new discontinuity preserving strategy has been developed to improve the accuracy of sparse unmixing by accounting for the spatial heterogeneity of endmember abundances (particularly at the edges of image objects). Our experimental results consistently show that the newly developed discontinuity preserving strategy for sparse unmixing can provide a better characterization of hyperspectral scenes by preserving the heterogeneity of abundance maps. Although the experimental results obtained in this paper are very encouraging, further experiments are required to fully substantiate our approach.

Table 1. SRE(dB) and p_s values(in brackets) achieved after applying different unmixing methods to the simulated data sets. The optimal parameters are reported.

SNR	SUnSAL	SUnSAL-DP	CLSUnSAL	CLSUnSAL-DP	SUnSAL-TV	SUnSAL-TV-DP
30	8.4007 (0.7905) $\lambda = 2e$-2	9.5427 (0.8725) $\lambda = 2e$-2	8.6458 (0.8029) $\lambda = 4e$-1	9.6777 (0.8923) $\lambda = 4e$-1	11.5332 (0.9608) $\lambda = 1e$-2 $\lambda_{TV} = 4e$-3	15.3295 (0.9988) $\lambda = 1e$-2 $\lambda_{TV} = 4e$-3
40	15.1565 (0.9882) $\lambda = 5e$-3	16.1805 (0.9914) $\lambda = 5e$-3	15.7865 (0.9888) $\lambda = 3e$-2	17.7295 (0.9990) $\lambda = 3e$-2	17.8147(1.0000) $\lambda = 5e$-3 $\lambda_{TV} = 1e$-3	21.4134 (1.0000) $\lambda = 5e$-3 $\lambda_{TV} = 1e$-3
50	23.1321 (1.0000) $\lambda = 1e$-3	24.4618 (1.0000) $\lambda = 1e$-3	26.0032 (1.0000) $\lambda = 2e$-2	28.5284(1.000) $\lambda = 2e$-2	26.1521 (1.0000) $\lambda = 2e$-3 $\lambda_{TV} = 2e$-4	28.3508 (1.000) $\lambda = 2e$-3 $\lambda_{TV} = 2e$-4

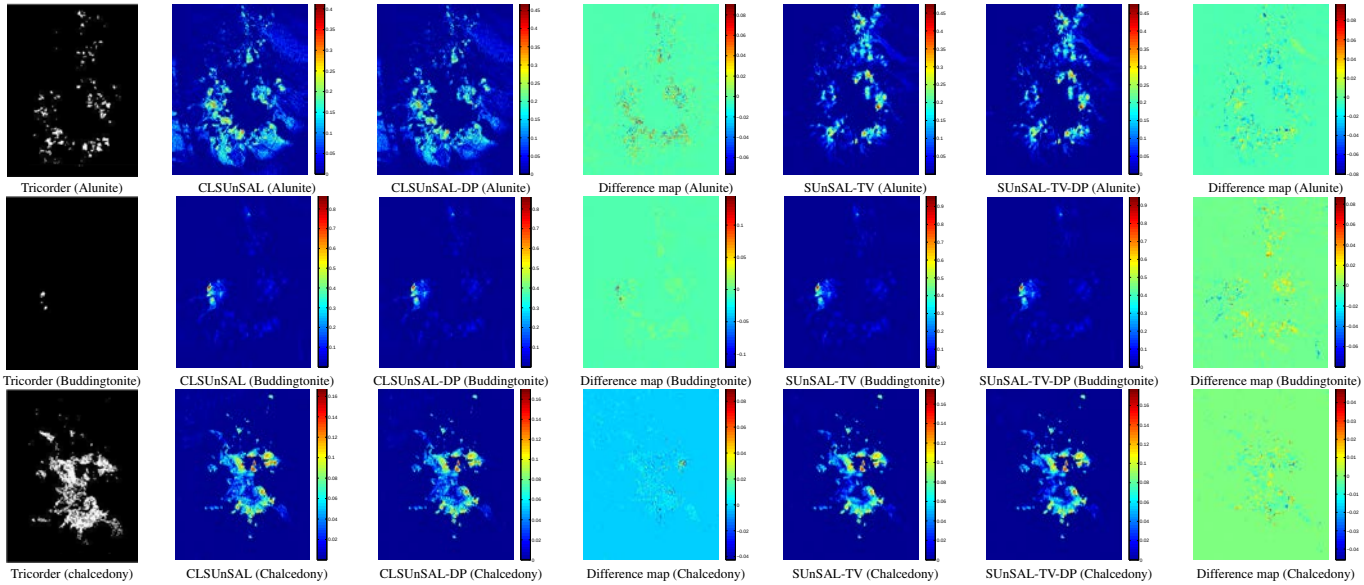

Fig. 4. Fractional abundance maps estimated by CLSUnSAL, SUnSAL-TV, CLSUnSAL-DP, and SUnSAL-TV-DP (as compared to the classification maps produced by USGS Tricorder software) for the considered 250×191 pixel subset of the AVIRIS Cuprite scene (and their difference maps).

7. REFERENCES

[1] J.M. Bioucas-Dias, A. Plaza, N. Dobigeon, M. Parente, Qian Du, P. Gader, and J. Chanussot, "Hyperspectral unmixing overview: Geometrical, statistical, and sparse regression-based approaches," *IEEE Journal of Selected Topics in Applied Earth Observations and Remote Sensing*, vol. 5, no. 2, pp. 354–379, Apr 2012.

[2] N. Keshava and J.F. Mustard, "Spectral unmixing," *IEEE Signal Processing Magazine*, vol. 19, no. 1, pp. 44–57, Jan 2002.

[3] M.-D. Iordache, J.M. Bioucas-Dias, and A. Plaza, "Sparse unmixing of hyperspectral data," *IEEE Transactions on Geoscience and Remote Sensing*, vol. 49, no. 6, pp. 2014–2039, Jun 2011.

[4] C. Shi and L. Wang, "Incorporating spatial information in spectral unmixing: A review," *Remote Sensing of Environment*, vol. 149, pp. 70–87, 2014.

[5] M.-D. Iordache, J.M. Bioucas-Dias, and A. Plaza, "Total variation spatial regularization for sparse hyperspectral unmixing," *IEEE Transactions on Geoscience and Remote Sensing*, vol. 50, no. 11, pp. 4484–4502, Nov 2012.

[6] O. Eches, N. Dobigeon, and J.-Y. Tourneret, "Enhancing hyperspectral image unmixing with spatial correlations," *IEEE Transactions on Geoscience and Remote Sensing*, vol. 49, no. 11, pp. 4239–4247, Nov 2011.

[7] L. Jimenez, J. Rivera-Medina, E. Rodriguez-Diaz, E. Arzuaga-Cruz, and M. Ramirez-Velez, "Integration of spatial and spectral information by means of unsupervised extraction and classification for homogenous objects applied to multispectral and hyperspectral data," *IEEE Transactions on Geoscience and Remote Sensing*, vol. 43, no. 4, pp. 844–851, April 2005.

[8] S. Jia and Y. Qian, "Constrained nonnegative matrix factorization for hyperspectral unmixing," *IEEE Transactions on Geoscience and Remote Sensing*, vol. 47, no. 1, pp. 161–173, Jan 2009.

[9] K. He, J. Sun, and X. Tang, "Guided image filtering," *IEEE Transactions on Pattern Analysis and Machine Intelligence*, vol. 35, no. 6, pp. 1397–1409, June 2013.

[10] X. Kang, S. Li, and J.A. Benediktsson, "Spectral-spatial hyperspectral image classification with edge-preserving filtering," *IEEE Transactions on Geoscience and Remote Sensing*, vol. 52, no. 5, pp. 2666–2677, May 2014.

[11] J. Li, M. Khodadadzadeh, A. Plaza, X. Jia, and J. M. Bioucas-Dias, "A discontinuity preserving relaxation scheme for spectral-spatial hyperspectral image classification," *IEEE Journal of Selected Topics in Applied Earth Observations and Remote Sensing*, vol. 9, no. 2, pp. 625–639, Feb 2016.

[12] M. Simoes, J.M. Bioucas-Dias, L. B Almeida, and J. Chanussot, "Hyperspectral image superresolution: An edge-preserving convex formulation," in *2014 IEEE International Conference on Image Processing (ICIP)*, 2014, pp. 4166–4170.

[13] E.J. Candès and T. Tao, "Decoding by linear programming," *IEEE Transactions on Information Theory*, vol. 51, no. 12, pp. 4203–4215, Dec 2005.

[14] M.-D. Iordache, J.M. Bioucas-Dias, and A. Plaza, "Collaborative sparse regression for hyperspectral unmixing," *IEEE Transactions on Geoscience and Remote Sensing*, vol. 52, no. 1, pp. 341–354, Jan 2014.

[15] R. Clark, G. Swayze, K. Livo, R. Kokaly, S. Sutley, J. Dalton, R. McDougal, and C. Gent, "Imaging spectroscopy: Earth and planetary remote sensing with the USGS Tetracorder and expert systems," *Journal of Geophysical Research*, vol. 108, no. E12, pp. 5131–5135, Dec 2003.